

INVESTIGATION OF IMPORTANT WEAK INTERACTION NUCLEI IN PRESUPERNOVA EVOLUTION

JAMEEL-UN NABI ^{1,2} ASIM ULLAH,¹ AND ALI ABAS KHAN³

¹*GIK Institute of Engineering Sciences and Technology, Topi 23640, KP, Pakistan*

²*University of Wah, Quaid Avenue, Wah Cantt 47040, Punjab, Pakistan*

³*FAST-National University of Computer and Emerging Sciences, Peshawar, KP, Pakistan*

ABSTRACT

The project aims to investigate most important weak interaction nuclei in the presupernova evolution of massive stars. To achieve the goal, an ensemble containing 728 nuclei in the mass range $A = 1-100$ was considered. We computed the mass fractions of these nuclei using Saha's equation for predetermined values of T , ρ and Y_e and assuming nuclear statistical equilibrium. The nuclear partition functions were obtained using a newly introduced recipe where excited states, up to 10 MeV, were treated as discrete. The weak interaction rates (electron capture (ec) and β -decay (bd)) were calculated in a *totally* microscopic fashion using the proton-neutron quasiparticle random phase approximation (pn-QRPA) model and without assuming the Brink-Axel hypothesis. The calculated rates were coupled with the computed mass fractions to investigate the time rate of change of lepton to baryon fraction of the stellar matter. We compare our results with the previous calculations reported in the literature. Noticeable differences up to orders of magnitude are reported with previous calculations. These differences may influence the evolution of the star in the later stages of presupernova. We present a list of top 50 ec and bd nuclei which have the largest effect on Y_e for conditions after silicon core burning. The competition between the ec and bd rates in stellar core was investigated and it was found that $Y_e = 0.424-0.455$ is the interval where the bd results are bigger than the ec rates.

Keywords: Nuclear Statistical Equilibrium, pn-QRPA, Electron Capture, β -Decay, Mass Fractions, Lepton to Baryon Fraction, Presupernova

1. INTRODUCTION

In the course of evolution of a massive star, weak interaction rates (β -decay (bd) and electron capture (ec)) play crucial roles. These reactions contribute to the gravitational collapse of the core of a massive star by reducing the electron degenerate pressure, thereby causing a supernova explosion and thus affect the formation of massive (neutron-rich) nuclei (Bethe et al. 1979; Bethe 1990).

Several attempts have been made for the calculation of weak interaction rates in stellar environment in a bid to have a better understanding of the stellar evolution. Fuller, Fowler, and Newman (FFN) (Fuller et al. 1980, 1982, 1985) employed the independent-particle model (IPM) using the then available experimental data and tabulated the weak interaction rates for 226 nuclei with mass in the range $60 \geq A \geq 21$. Their rates led to a considerable reduction in the lepton to baryon fraction (Y_e) throughout the stellar core and significantly contributed to a better understanding of the presupernova evolution of stars (Weaver et al. 1985). In 1994, Aufderheide and collaborators (Aufderheide et al. 1994) studied the influence of weak interaction in evolution of massive stars post silicon burning and searched for most important ec and bd nuclei in Y_e range of 0.400–0.500 using the IPM model. **They extended the FFN work for heavier nuclei with $A > 60$ and took into consideration explicit quenching of the GT strength.** In the same decade, many authors e.g. (Vetterli et al. 1989; El-Kateb et al. 1994; Williams et al. 1995) raised concern on the systematic parameterization employed by FFN and later adopted by Aufderheide et al. **The proton-neutron**

Corresponding author: Jameel-Un Nabi

jameel@giki.edu.pk

vc@uow.edu.pk

quasiparticle random phase approximation (pn-QRPA) (Nabi & Klapdor-Kleingrothaus 1999, 2004) and shell model (Langanke & Martínez-Pinedo 2000) later calculated weak interaction rates in stellar matter and showed that primarily the misplacement of the GT centroids by FFN in some key nuclei led to disagreement with experimental values. Heger and collaborators (Heger et al. 2001) utilized weak rates in the mass range $A = 45 - 65$ based on large-scale shell-model (LSSM) (Langanke & Martínez-Pinedo 2001) and performed simulation studies during the presupernova evolution. A similar study of the presupernova evolution using the pn-QRPA rates was not performed and was much awaited.

The aim of the current work is to search for the most important weak interaction nuclei in the presupernova evolution of massive stars using the pn-QRPA model. To achieve this goal, we considered a large pool containing 728 nuclei having atomic number up to 50 and mass number up to 100, in order to cover a decent number of nuclei prevailing in the stellar matter. The nuclei that contribute to largest change in Y_e values are neither the most abundant nor the ones with the strongest rates but a combination of the two. Thus one must know both the rates and nuclear abundance of nuclei to determine the most important weak interaction (ec or bd) nuclei for given values of T (temperature), ρ (baryon density) and Y_e . To compute ec and bd rates for the wide suite of selected nuclei, we employed the pn-QRPA (Halbleib Sr & Sorensen 1967) theory, a successful microscopic model frequently used in the past, with reasonable success, to compute the weak rates under terrestrial (Staudt et al. 1990; Hirsch et al. 1993) and stellar conditions (Nabi & Klapdor-Kleingrothaus 1999, 2004). The reliability of the pn-QRPA model was thoroughly discussed earlier (Nabi & Klapdor-Kleingrothaus 2004). A very decent comparison of pn-QRPA model calculation with experimental data was achieved for more than thousand nuclei (see Tables E–M and Figures 11–17 of (Nabi & Klapdor-Kleingrothaus 2004). For further comparison of pn-QRPA model with measured data please see Refs. (Majid & Nabi 2016; Majid et al. 2017; Nabi & Böyükata 2016; Nabi et al. 2015; Nabi & Bayram 2020)). The pn-QRPA model is much suitable for stellar rate calculations for the important reason that it does not assume the Brink-Axel hypothesis (Brink 1958) for computation of excited state GT strength distributions, as usually done in such calculations. Furthermore a large model space, up to seven major shells, makes the model calculation possible for any arbitrary heavy nucleus. Nuclear abundances were determined using the Saha’s equation assuming nuclear statistical equilibrium (NSE). We later investigate the total rate of change of Y_e with changing stellar conditions and also compare our results with previous calculations.

This paper is structured as follows: In Section 2 we briefly introduce the formalism employed to compute weak rates and nuclear abundances. Our results are discussed and compared with previous calculations in Section 3. Finally, concluding remarks are stated in the last section.

2. FORMALISM

2.1. Weak interaction rates

The ec and bd rates from the i th state of the parent to the j th state of the daughter nucleus in stellar matter is given by

$$\lambda_{ij} = \ln 2 \frac{\phi_{ij}^{ec(bd)}(T, \rho, E_f)}{(ft)_{ij}}. \quad (1)$$

In Eq. 1, $(ft)_{ij}$ is related to the reduced transition probability B_{ij} of the nuclear transition by

$$(ft)_{ij}^{ec(bd)} = D/B_{ij}, \quad (2)$$

where

$$B_{ij} = B(F)_{ij} + (g_A/g_V)^2 B(GT)_{ij}. \quad (3)$$

The value of constant D was taken as 6143 s (Hardy & Towner 2009) and the ratio of axial-vector and vector coupling constant was kept as $g_A/g_V = -1.2694$ (Nakamura 2010). $B(F)$ and $B(GT)$ are the reduced transition probabilities of the Fermi and GT transitions, respectively.

$$B(F)_{ij} = \frac{1}{2J_i + 1} |\langle j || \sum_k t_{\pm}^k || i \rangle|^2 \quad (4)$$

$$B(GT)_{ij} = \frac{1}{2J_i + 1} |\langle j || \sum_k t_{\pm}^k \vec{\sigma}^k || i \rangle|^2, \quad (5)$$

where J_i is the spin of parent state, $\vec{\sigma}$ are the Pauli spin matrices and t_{\pm} refer to the isospin raising and lowering operators.

The phase space function (ϕ_{ij}) is an integral over the total energy. For the case of bd , it is given by (here onwards we use natural units, $\hbar = m_e = c = 1$)

$$\phi_{ij} = \int_1^{\omega_m} \omega \sqrt{\omega^2 - 1} (\omega_m - \omega)^2 F(+Z, \omega) (1 - G_-) d\omega, \quad (6)$$

whereas the phase space for ec is given by

$$\phi_{ij} = \int_{\omega_l}^{\infty} \omega \sqrt{\omega^2 - 1} (\omega_m + \omega)^2 F(+Z, \omega) G_- d\omega, \quad (7)$$

where ω is the total energy of the electron including its rest mass, ω_l is the total capture threshold energy for ec and ω_m is the total bd energy. $\omega_m = (m_p - m_d + E_i - E_j)$ where $m_p(m_d)$ and $E_i(E_j)$ are the mass and excitation energies of the parent (daughter) nucleus. The $F(+Z, \omega)$ are the Fermi functions computed using the recipe of Gove and Martin (Gove & Martin 1971). G_- is the electron distribution function given by

$$G_- = [\exp(\frac{E - E_f}{kT}) + 1]^{-1}, \quad (8)$$

where $E = (\omega - 1)$ stands for kinetic energy of electrons and E_f is the Fermi energy of electrons.

The number density of protons associated with electrons and nuclei was determined using

$$\rho Y_e = \frac{1}{\pi^2 N_A} \left(\frac{m_e c}{\hbar}\right)^3 \int_0^{\infty} (G_- - G_+) p^2 dp, \quad (9)$$

where $p = (\omega^2 - 1)^{1/2}$ is lepton's momentum and G_+ is the positron distribution function

$$G_+ = [\exp(\frac{E + 2 + E_f}{kT}) + 1]^{-1}. \quad (10)$$

Due to prevailing high temperatures in stellar core, there is a finite probability of occupation of parent excited states. Hence weak decays have finite contribution from these states. Assuming thermal equilibrium, the probability of occupation of parent state i was estimated using

$$P_i = \frac{\exp(-E_i/kT)}{\sum_{i=1} \exp(-E_i/kT)}. \quad (11)$$

The total weak-decay rate per unit time per nucleus was finally computed using

$$\lambda^{ec(bd)} = \sum_{ij} P_i \lambda_{ij}^{ec(bd)}. \quad (12)$$

We considered 300 parent ad 300 daughter excited states in our rate calculation. The summation over the initial and final states was carried out until satisfactory convergence was achieved in the calculation. P_i is the probability of occupation of parent excited states and follows the normal Boltzmann distribution.

2.2. Nuclear abundances

During stellar evolution, once the silicon burning is completed, NSE can be achieved where strong and electromagnetic interactions are in equilibrium. The weak interaction is still not in equilibrium as the stellar matter is transparent to neutrinos produced and energy is channeled out of the system. In such a scenario, the isotropic abundances of nuclei follow simply from the nuclear Saha's equation for a given ρ , T and Y_e (Hartmann et al. 1985). We treated NSE in the same way it was previously employed by (Clifford & Tayler 1965; Kodama & Takahashi 1975; Hartmann et al. 1985).

According to Saha's equation, the nuclear abundance of k th nucleus is given by

$$\tau_k(A, Z) = \frac{C(A, Z, T)}{2} \left(\frac{\rho N_A \lambda_T^3}{2}\right)^{A-1} \times A^{\frac{5}{2}} \tau_n^{A-Z} \tau_p^Z \exp[Q_k(A, Z)/k_B T], \quad (13)$$

where $C(A,Z,T)$ is the nuclear partition function of the k th nucleus, N_A is the Avogadro's number, $\lambda_T (= \sqrt{\frac{h^2}{2\pi m_H k_B T}})$ is the thermal wavelength, Q_k is the ground state binding energy and k_B is the Boltzmann constant. τ_n and τ_p are the mass fractions of the free neutrons and protons, respectively, and can be determined subject to mass conservation

$$\sum_k \tau_k = 1 \quad (14)$$

and charge conservation

$$\sum_k \frac{Z_k}{A_k} \tau_k = Y_e = \frac{1 - \eta}{2}, \quad (15)$$

where η is the neutron excess. τ_k for k th nucleus can be calculated once τ_n and τ_p are determined. The time derivative of Y_e is a key parameter to be monitored during the presupernova evolution and for a k th nucleus it is given by

$$\dot{Y}_{e(k)}^{ec(bd)} = -(\pm) \frac{\tau_k}{A_k} \lambda_k^{ec(bd)}, \quad (16)$$

where the negative sign is for ec and positive for bd , A is the mass number and $\lambda^{ec(bd)}$ was calculated using Eq. 12.

While investigating isotopic abundances in presupernova cores (Dimarco et al. 2002) showed that the computed nuclear partition functions showed a deviation of up to 50% when low-lying nuclear states were considered as discrete energy levels as against those assuming a level density function and performing integrations. The authors were able to conduct a summation over states up to 3 MeV. Since the computed nuclear partition function is the cause of one of the biggest uncertainties in calculated mass fractions, Nabi and collaborators (Nabi et al. 2016a,b) recently introduced a novel recipe for an accurate description of nuclear partition functions which we follow here. The basic idea is to calculate discrete energy levels up to 10 MeV excitation energies. Beyond 10 MeV, a simple level density function was assumed and integration was performed up to 25 MeV excitation energy. In case few measured levels were missed in the process, they were inserted manually along with their spins in the calculation.

The nuclear partition function was calculated using

$$C(A, Z, T) = \sum_{\mu=0}^{\mu_m} (2J^\mu + 1) \exp[-E^\mu/kT] + \int_{E^{\mu_m}}^{E^{max}} \sum_{J^\mu, \pi^\mu} (2J^\mu + 1) \exp(-\epsilon/kT) \rho_l(\epsilon, J^\mu, \pi^\mu) d\epsilon, \quad (17)$$

where μ_m labels the last employed (either experimentally available or theoretically calculated) energy eigenstate. The first term in the above equation represents contribution from low-lying states (experimental or pn-QRPA predicted energy eigenvalues) up to E^μ and the sum runs over all Boltzmann-weighted states from ground state to μ_m . The second term uses process of integration to sum the contribution from continuous states. E^{max} was taken as 25 MeV. For details of the formalism we refer to (Nabi et al. 2016a,b).

3. RESULTS AND DISCUSSION

We employed the pn-QRPA model to compute the weak decay rates and mass fractions for our selected pool containing 728 nuclei in the mass range $A = 1-100$. It is worth mentioning that our pool of nuclei is significantly larger than the ones considered by previous studies. Recently the Gross Theory (Ferreira et al. 2014) was employed to estimate ec and bd rates under stellar conditions. We compared our calculation with the results of Gross Theory (referred to as GTh throughout the text) and the IPM calculation performed by (Aufderheide et al. 1994) and referred to as IPM onwards. Our selected pool of 728 nuclei may be compared with 150, 63 and around 100 nuclei chosen by IPM, GTh and SM (Langanke & Martinez-Pinedo 2000), respectively. A small pool of nuclei can omit few key nuclei which may dominate the nuclear composition during the late phases of the collapse before neutrino trapping. The number of nuclei in stellar ensemble may reach around 2700 species, as reported by the authors in Ref. (Juodagalvis et al. 2010). According to previous findings (Rauscher & Thielemann 2000; Rauscher 2003), calculation of partition functions is sensitive to the input mass models. All theoretical masses used in this project (including Q-values) were derived from the recent mass compilation of Audi et al. (Audi et al. 2017). For the cases where mass values were not given, we used Ref. (Möller et al. 2016) to compute the Q-values.

We estimated the rate of change of lepton to baryon fraction (\dot{Y}_e), separately for ec (Tables 1-3) and bd rates (Tables 4-6) and sorted 30 nuclei with largest contribution to \dot{Y}_e . The ec and bd rates, for all the nuclei listed in Tables 1-6, have been calculated using only allowed GT transitions. Our calculated weak rates and the corresponding \dot{Y}_e values

are, most of the times smaller than, sometimes bigger and at times comparable to the corresponding results of IPM. For example, our calculated ec rates are smaller than IPM rates by a factor of 4 for ^{50}V , ^{54}Fe and ^{64}Cu and factor 2 for ^{61}Co , ^{58}Co , ^{59}Ni and ^{63}Ni (see Table 1-3). Our bd rates are a factor 3, 4 and 5 bigger than IPM rates for ^{53}Ti , ^{66}Co and ^{65}Co , respectively (Table 4-6). The biggest difference between the two calculations were noted for ^{54}Mn and ^{62}Cu ($^{58,60}\text{Co}$), where our computed ec (bd) rates were found 2 (5) orders of magnitude smaller than IPM results. Similar differences were found for \dot{Y}_e values between the two models. Our computed total \dot{Y}_e (shown in the bottom of Tables 1-6) is always smaller than IPM value both at low and high (T_9 , ρ) values. **Misplacement of GT centroids** relative to experimental values led to bigger weak rates in majority of cases for IPM. When comparing our ec rates with those calculated by GTh, it is noted that *all* rates and the corresponding \dot{Y}_e values calculated by our model are bigger by orders of magnitude. Only in very few bd cases (^{49}Ca , ^{56}Mn and ^{60}Co), our computed rates and the respective \dot{Y}_e values are smaller than GTh. The GTh results include transitions *only* from ground state which clearly is a poor approximation to be used for stellar rate calculations. The pn-QRPA model included a huge model space of $7\hbar\omega$ to efficiently handle excited states in parent and daughter nuclei. Keeping in view the good comparison of pn-QRPA calculated values with measured data, our ground and excited state GT strength distributions depict a more realistic picture of the proceedings and contribute significantly to the reliability of our calculation. We again remind that Brink-Axel hypothesis was not used in computation of excited state GT strength functions in our calculation. Figure 1 shows our computed mass fractions for few abundant nuclei in NSE as a function of neutron excess (η) at different temperatures and densities. For the sake of comparison we used the same parameters (T_9 , ρ and η) as used in Figure 1 of IPM. It is noted that the computed mass fractions follow the same behavior in both models with slight variations. The different recipes for nuclear partition functions and different mass models in the two approaches resulted in this small difference. We believe that using our recipe of nuclear partition functions would lead to a more reliable computation of mass fractions (see also (Nabi et al. 2016b) for detailed analysis of the comparison between the two computed mass fractions).

Figure 2 compares our computed ec (upper panel) and bd (lower panel) rates as a function of Y_e with the GTh results. The ec rates are sensitive to the stellar temperature and density values, showing an increase for higher values of T_9 and ρ . The behavior of our computed weak rates as a function of Y_e is also in agreement with IPM i.e. the ec rates approaching higher values when the magnitude of Y_e is reduced (T_9 and ρ increased) while there is a decrease in bd rates when the Y_e is decremented. The electron chemical potential increases with rise in stellar density and that is why the ec rates are enhanced at lower Y_e values. For higher density, the enhanced chemical potential of electron outside the nuclei impede the bd rates. The major reduction in the density ($4\text{E}+10$ to $1\text{E}+9$) g/cm^3 accounts for the sudden increase (decrease) in the bd (ec) rates in the short interval of $Y_e = 0.410-0.430$. The slope of the graph is relatively less steep for higher Y_e values because of the smooth reduction in the T_9 and ρ values. Our computed weak rates are bigger by as much as 1–2 orders of magnitude when compared with those of GTh results for the cases shown in Figure 2. The reasons for our bigger rates were discussed above. Figure 3 depicts our computed ec rates, as a function of Y_e , for Ni, Co, Cu and Mn isotopes while Figure 4 shows our bd rates for Fe, Co, Ni and Mn isotopes.

The evolution of rate of change of lepton to baryon fraction (\dot{Y}_e) is shown in Figure 5. Panel (a) depicts 15 nuclei with largest contribution to the total \dot{Y}_e values for ec , whereas panel (b) shows similar results for 10 nuclei having higher \dot{Y}_e values for bd . Figure 6 shows the sum of \dot{Y}_e values for both ec and bd rates. Here we compare our results with three other models namely IPM, GTh and SM. It can be seen from Figures 5-6 that the ec rates dominate toward the end values of our chosen range of Y_e , while the bd rates win somewhere at the center value ($Y_e \approx 0.440$). At $Y_e = 0.410$, the contribution of ^{67}Ni , ^{83}As and ^{79}Ge to the total \dot{Y}_e^{ec} is greater than the contribution of ^{49}Ca , ^{63}Fe and ^{51}Sc to the \dot{Y}_e^{bd} and hence the ec rates are dominant at this point. The \dot{Y}_e^{ec} decreases and \dot{Y}_e^{bd} increases with rise in Y_e values up to $Y_e \approx 0.422$. However the ec rates are still dominant. With further increase in the Y_e value beyond 0.422, though the contribution of \dot{Y}_e^{ec} for ^{67}Cu , ^{56}Mn and ^{51}Ti is bigger, once the share of other key bd nuclei are summed up, the total \dot{Y}_e^{ec} is smaller than the corresponding \dot{Y}_e^{bd} . The increase (decrease) in \dot{Y}_e^{bd} (\dot{Y}_e^{ec}) continues till $Y_e = 0.440$ (0.455). Beyond $Y_e \approx 0.440$, where the density is $3.30\text{E}+8$ g/cm^3 and temperature is around $4.24\text{E}+9$ K , the \dot{Y}_e^{bd} starts to decrease but still dominates up to values of $Y_e \approx 0.455$ due to main contribution coming from ^{63}Co and ^{51}Ti . The decrease in bd continues till end point ($Y_e \approx 0.500$) whereas the ec continues growing beyond $Y_e \approx 0.455$ with major contribution coming from ^{55}Fe , $^{56-58}\text{Ni}$ and ^{55}Co . The bd remains dominant over ec for the interval $Y_e \approx 0.424-0.455$, 11% greater than the one proposed by IPM ($Y_e \approx 0.425-0.453$). Our proposed interval was found close to the SM and GTh intervals, which were $Y_e \approx 0.42-0.46$ and $Y_e \approx 0.422-0.455$, respectively. It may be seen from Fig. 6 that our estimated total $\dot{Y}_e^{ec(bd)}$ values are smaller in magnitude than IPM results, bigger than GTh estimations and

in good agreement with the SM estimation. The end result necessitates the use of a microscopic model for calculation of stellar weak rates.

We finally determined the most important weak interaction nuclei that have the largest effect on Y_e post silicon core burning, by averaging the contribution from each nucleus to \dot{Y}_e over the entire chosen stellar trajectory. To this effect we introduced a ranking parameter (\mathring{R}_p) given by

$$\mathring{R}_p = \left(\frac{\dot{Y}_{e(k)}^{ec(bd)}}{\sum \dot{Y}_{e(k)}^{ec(bd)}} \right)_{0.500 > Y_e > 0.400} \quad (18)$$

Thus, nuclei with largest contribution to \dot{Y}_e will have the highest value of \mathring{R}_p . On the basis of \mathring{R}_p , we listed top 50 *ec* and *bd* nuclei for all conditions which follow silicon core burning in Table 7. It is worth noting that 90% (70%) of our most important *ec* (*bd*) nuclei are the same as the list provided by IPM. The nuclei marked with an asterisk are the ones missing in the list provided by the IPM.

4. CONCLUDING REMARKS

In this work we present the first ever compilation of nuclei which have the largest effect on Y_e for conditions after silicon core burning using the pn-QRPA model. The use of a fully microscopic model adds to the reliability of calculated weak rates. The pn-QRPA model does not employ the Brink-Axel hypothesis for calculation of excited state GT strength distributions – a feature not available even in the large scale shell model calculation. We are currently working on quantifying the disadvantages of employing Brink-Axel hypothesis for calculation of stellar rates and hope to report our findings soon. The reliability of pn-QRPA results and its decent comparison with measured data were discussed in Section 1. Our computation of mass abundances also used a novel recipe for calculation of nuclear partition functions. We considered all excited states up to 10 *MeV* as discrete which may result in a more realistic calculation of isotopic abundances according to a previous study.

Our results are shown in Tables 1-7 which show rankings of nuclei during several key snapshots of presupernova evolution of massive stars. Specially Table 7 presents an overall ranking for all conditions post silicon burning phase and we compile a list of top 50 *ec* and *bd* nuclei causing largest effect on Y_e . It is to be noted that the list contains 10% of new *ec* and 30% of new *bd* nuclei not to be seen in the list of IPM tables. **For a nucleus with $A \sim 100$ at $T_9 = 5.39$ GK, the mean nuclear excitation energy is ~ 3 MeV and transitions above 10 MeV excitation is in order. Our nuclear partition function (Eq. 17) considers discrete states only up to 10 MeV. Beyond 10 MeV we assumed a level density function and this may bear consequences for the calculated mass fractions.** Core-collapse simulators may find this updated list interesting for their future studies. This list can further be extended to top 700 nuclei and may be requested from the corresponding author.

Another key finding of this paper is that we propose an updated interval $Y_e = 0.424-0.455$ in which the *bd* rates dominate the competing *ec* rates which is roughly 11% bigger than proposed by IPM and 6% smaller than GTh range. Further our estimated total $\dot{Y}_e^{ec(bd)}$ values are in good agreement with shell model prediction. We plan to extend our pool of nuclei with $A > 100$ and explore role of forbidden transitions (that become important for neutron-rich matter) in the list of nuclei having largest effect on Y_e in the near future.

5. ACKNOWLEDGMENTS

J.-U. Nabi would like to acknowledge the support of the Higher Education Commission Pakistan through project numbers 5557/KPK /NRPU/R&D/HEC/2016 and 9-5(Ph-1-MG-7)/PAK-TURK /R&D/HEC/2017.

Table 1. The ec rates for most important nuclei sorted in order of $|\dot{Y}_e^{ec}|$. The rates are compared with IPM and GTh results wherever available. The units of ρ , T_9 , λ^{ec} and \dot{Y}_e^{ec} are g/cm^3 , GK , s^{-1} and s^{-1} , respectively.

		$\rho = 1.06E+09,$			$T_9 = 4.93,$			$Y_e = 0.430$		
		λ_k^{ec}			$ \dot{Y}_{e(k)}^{ec} $					
A	Symbol	pn-QRPA	IPM	GTh	pn-QRPA	IPM	GTh			
67	Cu	3.54E-02	2.38E-03	—	2.33E-06	2.26E-07	—			
66	Cu	4.63E-01	6.56E-01	—	1.47E-06	1.30E-06	—			
52	V	5.64E-02	1.81E-02	1.17E-05	7.05E-07	2.58E-07	1.16E-08			
56	Mn	7.91E-02	2.90E-02	2.61E-04	5.88E-07	2.91E-07	1.28E-08			
60	Co	7.69E-01	2.31E+00	4.27E-03	5.65E-07	3.66E-06	1.80E-08			
49	Sc	1.94E-03	—	—	2.63E-07	—	—			
65	Cu	1.08E-01	5.91E-02	—	1.43E-07	1.67E-07	—			
62	Co	9.31E-03	3.22E-02	2.75E-05	1.26E-07	5.34E-07	1.69E-09			
54	Cr	6.41E-05	—	—	7.10E-08	—	—			
49	Ti	6.41E-02	1.70E-02	—	5.67E-08	4.09E-08	—			
53	Cr	5.16E-03	—	—	5.13E-08	—	—			
51	Ti	1.08E-04	—	—	5.13E-08	—	—			
51	V	6.34E-03	9.71E-03	1.67E-04	4.87E-08	1.53E-07	2.32E-09			
63	Ni	1.92E-03	3.87E-03	—	4.51E-08	8.15E-08	—			
64	Ni	2.10E-05	—	—	4.25E-08	—	—			
48	Sc	8.34E-02	8.25E-02	—	4.05E-08	1.02E-07	—			
57	Mn	5.78E-04	4.03E-04	—	3.83E-08	6.33E-08	—			
61	Co	1.09E-03	2.23E-03	—	3.79E-08	2.42E-07	—			
68	Cu	2.18E-03	2.62E-02	—	3.66E-08	3.21E-07	—			
55	Cr	1.66E-04	—	—	2.51E-08	—	—			
73	Ga	4.58E-03	—	—	2.26E-08	—	—			
59	Fe	1.36E-04	1.83E-04	—	1.92E-08	4.51E-08	—			
53	V	2.74E-04	—	—	1.90E-08	—	—			
50	Sc	1.03E-03	—	—	1.83E-08	—	—			
72	Ga	2.82E-02	—	—	1.74E-08	—	—			
65	Ni	4.65E-05	—	—	1.61E-08	—	—			
71	Ga	3.45E-02	—	—	1.53E-08	—	—			
55	Mn	3.50E-03	8.73E-03	4.26E-05	1.43E-08	7.70E-08	5.53E-10			
69	Zn	1.06E-02	—	—	1.37E-08	—	—			
58	Fe	3.27E-05	—	—	1.27E-08	—	—			
		$\sum \dot{Y}_e^{ec} \rightarrow$			-1.01E-06	-8.21E-06	-4.89E-08			

Table 2. Same as Table 1 but at conditions given below.

		$\rho = 1.45\text{E}+08,$	$T_9 = 3.8,$		$Y_e = 0.450$		
		λ_k^{ec}			$ \dot{Y}_{e(k)}^{ec} $		
A	Symbol	pn-QRPA	IPM	GTh	pn-QRPA	IPM	GTh
60	Co	1.04E-02	1.27E-02	2.76E-05	3.48E-08	1.27E-07	9.41E-10
59	Co	4.63E-04	6.57E-04	4.35E-08	2.41E-08	1.27E-07	7.60E-12
61	Ni	9.79E-04	1.20E-03	3.72E-07	9.23E-09	2.86E-08	2.20E-11
53	Mn	9.98E-03	8.97E-03	—	8.16E-09	1.37E-08	—
64	Cu	8.65E-02	3.69E-01	—	6.41E-09	4.25E-08	—
55	Fe	4.38E-03	6.00E-03	3.54E-04	5.68E-09	1.25E-08	1.23E-09
58	Co	1.69E-02	3.07E-02	4.00E-04	4.52E-09	1.48E-08	1.83E-09
56	Fe	2.24E-06	1.31E-06	—	3.74E-09	1.93E-09	—
57	Fe	2.33E-05	1.84E-05	—	3.32E-09	3.82E-09	—
63	Cu	1.00E-02	1.86E-02	9.89E-11	3.12E-09	1.53E-08	9.59E-11
55	Mn	1.26E-05	2.25E-05	—	2.56E-09	1.21E-08	—
53	Cr	8.47E-06	2.46E-06	—	1.77E-09	9.57E-10	—
51	Cr	3.09E-02	9.33E-03	8.47E-04	1.37E-09	1.36E-09	2.94E-10
54	Mn	4.06E-04	1.57E-02	—	1.33E-09	6.68E-08	—
65	Cu	5.75E-04	—	—	1.24E-09	—	—
57	Co	3.92E-03	1.29E-02	5.40E-04	7.59E-10	8.67E-09	4.97E-10
51	V	1.53E-05	2.96E-05	—	7.02E-10	3.45E-09	—
49	Ti	4.40E-04	—	—	4.12E-10	—	—
52	Cr	3.80E-07	—	—	2.89E-10	—	—
60	Ni	4.15E-06	2.74E-05	—	2.67E-10	1.53E-09	—
49	V	1.34E-01	—	—	2.54E-10	—	—
50	V	5.35E-03	2.45E-02	1.36E-03	2.10E-10	2.60E-09	8.31E-10
56	Mn	3.08E-05	2.56E-04	3.36E-09	2.06E-10	3.22E-09	2.88E-13
59	Ni	7.55E-03	—	1.17E-03	1.83E-10	—	1.46E-10
62	Cu	3.02E-01	4.60E+00	1.07E-03	1.82E-10	3.77E-09	1.07E-11
62	Ni	3.62E-08	—	—	9.63E-11	—	—
61	Cu	5.66E-01	—	2.02E-03	7.55E-11	—	1.64E-12
48	V	1.26E+02	—	—	7.28E-11	—	—
63	Ni	2.06E-06	—	—	5.73E-11	—	—
54	Fe	6.79E-04	—	—	4.76E-11	—	—
$\sum \dot{Y}_e^{ec} \rightarrow$					-2.55E-08	-4.96E-07	-5.91E-09

Table 3. Same as Table 1 but at conditions given below.

		$\rho = 5.86\text{E}+07,$			$T_9 = 3.40,$			$Y_e = 0.470$		
		λ_k^{ec}			$ \dot{Y}_{e(k)}^{ec} $					
A	Symbol	pn-QRPA	IPM	GTh	pn-QRPA	IPM	GTh	pn-QRPA	IPM	GTh
58	Ni	6.10E-04	6.36E-04	7.42E-06	6.39E-07	5.97E-07	2.45E-08			
55	Fe	1.09E-03	1.61E-03	5.01E-05	5.71E-07	1.52E-06	1.14E-07			
53	Mn	3.27E-03	2.48E-03	—	3.95E-07	6.09E-07	—			
55	Co	1.25E-01	1.41E-01	1.68E-03	3.89E-07	1.37E-06	1.73E-07			
54	Fe	8.61E-05	3.11E-04	—	3.74E-07	1.21E-06	—			
57	Co	1.94E-03	3.50E-03	9.35E-05	3.07E-07	2.18E-06	1.25E-07			
57	Ni	5.47E-02	1.94E-02	5.94E-03	1.40E-07	5.84E-08	2.45E-07			
56	Co	2.64E-02	7.40E-02	1.68E-03	1.23E-07	7.35E-07	1.89E-07			
59	Ni	2.17E-03	4.37E-03	2.41E-04	8.81E-08	3.80E-07	8.69E-08			
61	Cu	1.35E-01	3.93E-01	4.96E-04	4.00E-08	3.22E-07	1.83E-09			
51	Cr	8.99E-03	2.81E-03	1.44E-04	1.71E-08	1.97E-08	3.61E-09			
48	V	3.47E+01	—	—	1.50E-08	—	—			
56	Ni	2.01E-02	1.60E-02	1.98E-03	1.17E-08	7.76E-09	2.66E-08			
58	Co	9.98E-03	1.04E-02	9.73E-05	1.09E-08	2.35E-08	2.60E-09			
53	Fe	5.73E-02	2.04E-02	—	7.90E-09	9.70E-09	—			
52	Mn	2.13E-02	2.85E-02	—	5.45E-09	1.62E-08	—			
50	Cr	1.67E-04	—	—	3.04E-09	—	—			
59	Cu	1.69E+00	1.01E+00	—	2.99E-09	4.62E-09	—			
54	Mn	6.93E-04	5.13E-03	—	1.87E-09	2.05E-08	—			
56	Fe	1.06E-07	—	—	9.98E-10	—	—			
49	V	3.51E-02	—	—	7.78E-10	—	—			
62	Cu	6.14E-02	1.59E+00	—	4.70E-10	1.85E-08	—			
60	Cu	2.02E-01	8.39E-01	4.07E-03	3.92E-10	4.30E-09	3.30E-10			
60	Ni	2.30E-07	1.49E-06	—	3.61E-10	2.21E-09	—			
51	Mn	1.43E-02	—	—	3.45E-10	—	—			
62	Zn	2.05E-02	—	—	1.66E-10	—	—			
52	Fe	1.50E-02	—	—	1.54E-10	—	—			
49	Cr	3.67E-02	—	—	8.31E-11	—	—			
61	Ni	8.20E-05	—	—	7.02E-11	—	—			
64	Zn	7.76E-04	—	—	6.95E-11	—	—			
$\sum \dot{Y}_e^{ec} \rightarrow$					-3.15E-06	-8.21E-06	-9.96E-07			

Table 4. Same as Table 1 but for bd and at conditions given below.

		$\rho = 2.20\text{E}+09,$			$T_9 = 5.39,$			$Y_e = 0.425$		
		λ_k^{bd}			$ \dot{Y}_{e(k)}^{bd} $					
A	Symbol	pn-QRPA	IPM	GTh	pn-QRPA	IPM	GTh	pn-QRPA	IPM	GTh
65	Co	1.75E-01	8.17E-02	—	2.81E-06	4.40E-06	—			
51	Sc	2.00E-01	3.44E-02	3.64E-03	1.38E-06	1.02E-06	8.66E-07			
53	Ti	4.03E-02	1.47E-02	7.14E-04	1.24E-06	1.07E-06	8.66E-08			
49	Ca	9.02E-03	9.31E-03	1.22E-03	1.07E-06	1.14E-06	3.91E-07			
66	Co	1.43E+00	3.24E-01	—	9.24E-07	1.01E-06	—			
62	Fe	2.66E-03	9.63E-03	—	7.21E-07	2.51E-06	—			
59	Mn	2.02E-02	1.39E-01	2.06E-04	6.51E-07	7.93E-06	3.03E-08			
67	Ni	6.53E-04	4.02E-03	7.88E-06	6.26E-07	2.85E-06	7.85E-09			
64	Co	1.98E-02	1.14E-01	—	5.58E-07	2.56E-06	—			
58	Cr	2.92E-02	1.64E-01	—	5.45E-07	5.03E-06	—			
77	Ga	4.98E-02	—	—	5.21E-07	—	—			
57	Cr	1.85E-02	1.20E-01	—	4.90E-07	9.17E-06	—			
63	Fe	9.84E-02	3.54E-01	1.47E-02	4.36E-07	1.61E-06	4.27E-07			
67	Co	3.24E+00	—	—	3.97E-07	—	—			
50	Sc	6.41E-03	5.54E-02	4.19E-03	3.31E-07	5.16E-06	1.44E-05			
60	Mn	5.71E-02	3.38E-01	7.78E-03	2.82E-07	1.22E-06	3.92E-08			
51	Ti	5.02E-04	—	—	2.60E-07	—	—			
71	Cu	4.33E-02	—	—	2.39E-07	—	—			
61	Fe	1.63E-03	3.54E-02	—	1.70E-07	8.50E-06	—			
68	Ni	1.93E-04	—	—	1.67E-07	—	—			
54	V	1.01E-02	6.08E-02	4.05E-03	1.56E-07	1.87E-06	2.72E-07			
49	Sc	8.20E-04	—	—	1.55E-07	—	—			
52	Sc	6.44E-01	—	—	1.27E-07	—	—			
63	Co	1.27E-03	5.27E-03	—	1.27E-07	1.58E-06	—			
75	Ga	2.82E-03	—	—	1.20E-07	—	—			
72	Cu	3.94E-01	—	—	1.12E-07	—	—			
55	V	9.82E-03	—	—	1.11E-07	—	—			
52	Ti	1.70E-04	4.49E-04	—	1.10E-07	2.69E-07	—			
56	V	4.61E-01	—	—	1.09E-07	—	—			
69	Ni	6.95E-03	—	—	1.08E-07	—	—			
$\sum Y_e^{bd} \rightarrow$					1.59E-05	6.87E-5	3.16E-06			

Table 5. Same as Table 1 but for bd and at conditions given below.

		$\rho = 3.30\text{E}+08,$			$T_9 = 4.24,$			$Y_e = 0.440$		
		λ_k^{bd}			$ \dot{Y}_{e(k)}^{bd} $					
A	Symbol	pn-QRPA	IPM	GTh	pn-QRPA	IPM	GTh	pn-QRPA	IPM	GTh
67	Ni	2.62E-02	1.20E-02	5.29E-04	8.52E-06	1.05E-07	5.70E-09			
49	Sc	3.55E-02	—	—	2.00E-06	—	—			
63	Co	3.16E-02	1.41E-02	3.52E-04	1.41E-06	7.46E-07	2.00E-08			
50	Sc	3.08E-01	1.79E-01	4.10E-02	1.21E-06	2.08E-07	2.04E-07			
65	Co	7.46E-01	1.39E-01	—	1.06E-06	2.02E-08	—			
59	Mn	1.44E-01	1.58E-01	5.40E-03	8.79E-07	2.89E-07	3.20E-08			
64	Co	2.68E-01	2.05E-01	—	8.62E-07	5.42E-08	—			
58	Cr	4.04E-01	2.79E-01	—	7.47E-07	2.88E-08	—			
69	Cu	3.53E-02	—	—	5.90E-07	—	—			
61	Fe	1.57E-02	6.44E-02	7.45E-04	5.29E-07	1.36E-06	3.45E-08			
51	Ti	1.76E-03	7.13E-04	—	4.32E-07	1.40E-07	—			
57	Cr	1.01E-01	1.49E-01	—	3.66E-07	2.00E-07	—			
62	Fe	2.75E-03	4.72E-02	—	2.70E-07	2.90E-07	—			
51	Sc	8.65E-01	1.32E-01	4.73E-02	2.37E-07	6.16E-09	8.17E-07			
55	Cr	2.79E-03	1.06E-03	1.12E-05	2.19E-07	2.49E-07	5.57E-09			
71	Cu	7.33E-01	—	—	1.45E-07	—	—			
63	Fe	5.82E-01	—	1.68E-01	1.12E-07	—	5.33E-09			
53	Ti	3.92E-02	3.19E-02	1.95E-02	1.02E-07	1.04E-08	1.24E-08			
49	Ca	1.39E-02	4.18E-02	2.84E-02	9.42E-08	7.27E-09	1.35E-08			
54	V	5.38E-02	1.90E-01	3.85E-02	8.67E-08	2.04E-07	1.15E-07			
75	Ga	3.21E-02	—	—	8.41E-08	—	—			
60	Mn	3.82E-01	—	—	7.83E-08	—	—			
70	Cu	3.34E-01	—	—	7.73E-08	—	—			
57	Mn	2.37E-03	5.32E-04	—	7.68E-08	8.02E-08	—			
58	Mn	1.14E-02	1.39E-01	5.80E-08	7.32E-08	6.30E-07	8.70E-08			
53	V	2.26E-03	2.98E-03	8.82E-05	6.64E-08	2.63E-07	2.05E-08			
55	V	5.83E-02	8.52E-02	—	5.19E-08	1.97E-08	—			
54	Ti	1.33E-01	—	—	4.41E-08	—	—			
65	Ni	1.71E-04	2.49E-03	—	4.22E-08	5.36E-07	—			
56	Cr	8.32E-05	1.14E-04	—	4.17E-08	2.01E-08	—			
					$\sum Y_e^{bd} \rightarrow$	2.08E-06	1.01E-05	6.39E-07		

Table 6. Same as Table 1 but for bd and at conditions given below.

		$\rho = 3.86\text{E}+07,$			$T_9 = 3.40,$			$Y_e = 0.470$		
		λ_k^{bd}			$ \dot{Y}_{e(k)}^{bd} $					
A	Symbol	pn-QRPA	IPM	GTh	pn-QRPA	IPM	GTh	pn-QRPA	IPM	GTh
55	Mn	1.08E-07	3.68E-07	—	1.78E-13	1.75E-12	—			
57	Fe	3.34E-08	1.10E-05	—	9.45E-14	5.04E-11	—			
58	Fe	2.90E-08	1.09E-07	—	4.14E-14	1.55E-13	—			
52	V	8.71E-03	1.60E-02	4.32E-04	3.93E-14	1.33E-13	2.76E-14			
53	Cr	3.75E-08	5.93E-06	—	2.55E-14	8.22E-12	—			
54	Cr	2.02E-07	2.90E-07	—	1.70E-14	2.46E-14	—			
59	Co	3.86E-09	8.11E-08	—	8.90E-15	7.69E-13	—			
61	Co	2.86E-04	1.36E-03	—	5.01E-15	1.02E-13	—			
57	Mn	7.43E-03	—	2.97E-05	4.24E-15	—	1.72E-16			
56	Fe	4.32E-13	1.19E-10	—	4.08E-15	1.07E-12	—			
54	Mn	1.12E-09	8.81E-06	—	3.01E-15	3.52E-11	—			
53	Mn	1.76E-11	—	—	2.12E-15	—	—			
56	Mn	7.41E-06	1.09E-02	2.37E-04	1.24E-15	3.87E-12	4.23E-13			
55	Cr	4.84E-03	—	—	1.04E-15	—	—			
60	Co	2.03E-06	4.66E-03	4.93E-05	1.03E-15	7.94E-12	2.17E-13			
52	Cr	1.48E-12	—	—	9.19E-16	—	—			
59	Fe	4.28E-05	6.95E-03	7.29E-07	6.66E-16	2.43E-13	1.15E-17			
57	Co	2.27E-12	1.34E-09	—	3.59E-16	8.36E-13	—			
51	V	5.96E-09	—	—	2.87E-16	—	—			
55	Fe	5.01E-13	1.30E-10	—	2.61E-16	1.23E-13	—			
51	Cr	1.05E-10	—	—	1.99E-16	—	—			
53	V	6.95E-03	—	—	5.39E-17	—	—			
49	Ti	1.96E-07	—	—	4.94E-17	—	—			
61	Ni	5.09E-11	—	—	4.36E-17	—	—			
51	Ti	2.89E-03	—	—	3.68E-17	—	—			
63	Ni	4.50E-07	3.16E-04	—	3.53E-17	2.90E-14	—			
58	Co	2.96E-11	5.67E-06	—	3.22E-17	1.27E-11	—			
50	V	7.87E-09	1.89E-05	3.2E-09	2.38E-17	1.79E-13	2.06E-16			
49	Sc	8.30E-02	—	—	2.31E-17	—	—			
62	Ni	7.36E-12	—	—	2.07E-17	—	—			
					$\sum Y_e^{bd} \rightarrow$	4.30E-13	1.24E-10	6.68E-13		

Table 7. List of top 50 most important *ec* and *bd* nuclei averaged throughout the stellar trajectory for $0.500 > Y_e > 0.400$. The ranking parameter \dot{R}_p is defined in text. Nuclei marked with asterisk are new entries not to be seen in the list compiled by IPM.

<i>ec</i> nuclei			<i>bd</i> nuclei								
A	Symbol	\dot{R}_p	A	Symbol	\dot{R}_p	A	Symbol	\dot{R}_p	A	Symbol	\dot{R}_p
56	Mn	1.11E+01	69	Cu	3.69E-02	67	Ni	5.34E-01	63	Fe*	1.39E-02
52	V	6.32E-01	54	Cr	3.63E-02	49	Sc*	1.33E-01	66	Co	1.35E-02
67	Cu	5.57E-01	81	Ge*	3.39E-02	65	Co	1.03E-01	58	Fe	1.24E-02
60	Co	4.03E-01	78	Ga	3.37E-02	63	Co	9.17E-02	71	Cu*	1.22E-02
53	Mn	2.51E-01	64	Cu	3.22E-02	50	Sc	8.56E-02	50	Ca	1.11E-02
49	Sc	2.40E-01	57	Co	3.19E-02	59	Mn	6.70E-02	60	Mn	8.93E-03
66	Cu	2.09E-01	63	Cu	3.04E-02	53	Mn*	6.56E-02	77	Ga*	8.82E-03
50	Sc	1.75E-01	58	Ni	3.02E-02	64	Co	6.50E-02	54	V	8.20E-03
55	Fe	1.68E-01	57	Fe	2.96E-02	49	Ca*	6.39E-02	53	Cr	7.87E-03
59	Co	1.53E-01	77	Ge	2.88E-02	55	Mn	5.64E-02	75	Ga*	6.91E-03
79	Ge	1.11E-01	64	Ni	2.79E-02	58	Cr*	5.47E-02	79	Ga*	6.23E-03
77	Ga	7.89E-02	58	Co	2.76E-02	69	Cu*	3.73E-02	70	Cu*	6.06E-03
61	Ni	7.60E-02	83	Se	2.73E-02	61	Fe	3.66E-02	54	Cr	5.92E-03
78	Ge*	7.46E-02	53	Cr	2.62E-02	51	Ti	3.54E-02	56	Fe	5.87E-03
83	As	6.85E-02	48	Sc*	2.57E-02	51	Sc	3.27E-02	53	V	5.84E-03
51	Ti	6.78E-02	51	Cr	2.51E-02	57	Fe	3.12E-02	58	Mn	5.11E-03
67	Ni	6.67E-02	65	Ni	2.48E-02	57	Cr	3.08E-02	55	V	4.90E-03
56	Ni	6.17E-02	55	Cr	2.40E-02	55	Cr	2.79E-02	51	Ca	4.88E-03
68	Cu	4.62E-02	64	Co	2.31E-02	62	Fe	2.66E-02	54	Ti	4.66E-03
82	As	4.60E-02	57	Mn	2.26E-02	57	Mn	2.42E-02	61	Co	4.63E-03
56	Fe	4.55E-02	71	Cu	2.23E-02	57	Co*	2.14E-02	51	Cr*	4.25E-03
65	Cu	4.48E-02	55	Mn	2.07E-02	53	Ti	2.12E-02	68	Ni	3.96E-03
55	Co	4.03E-02	53	V	2.05E-02	52	V	1.80E-02	56	Cr	3.70E-03
75	Ga*	3.83E-02	73	Ga*	2.03E-02	55	Fe*	1.78E-02	68	Co	3.65E-03
57	Ni	3.69E-02	51	V	1.96E-02	67	Co*	1.44E-02	54	Mn	3.37E-03

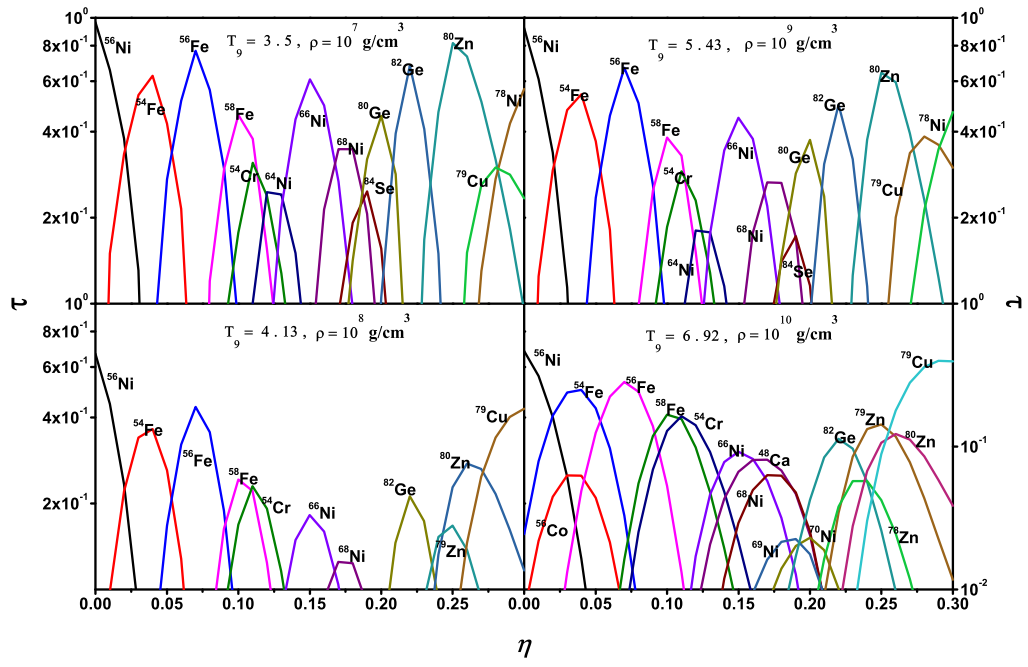


Figure 1. Mass fractions of some abundant nuclei in NSE as a function of neutron excess, at different densities and temperatures.

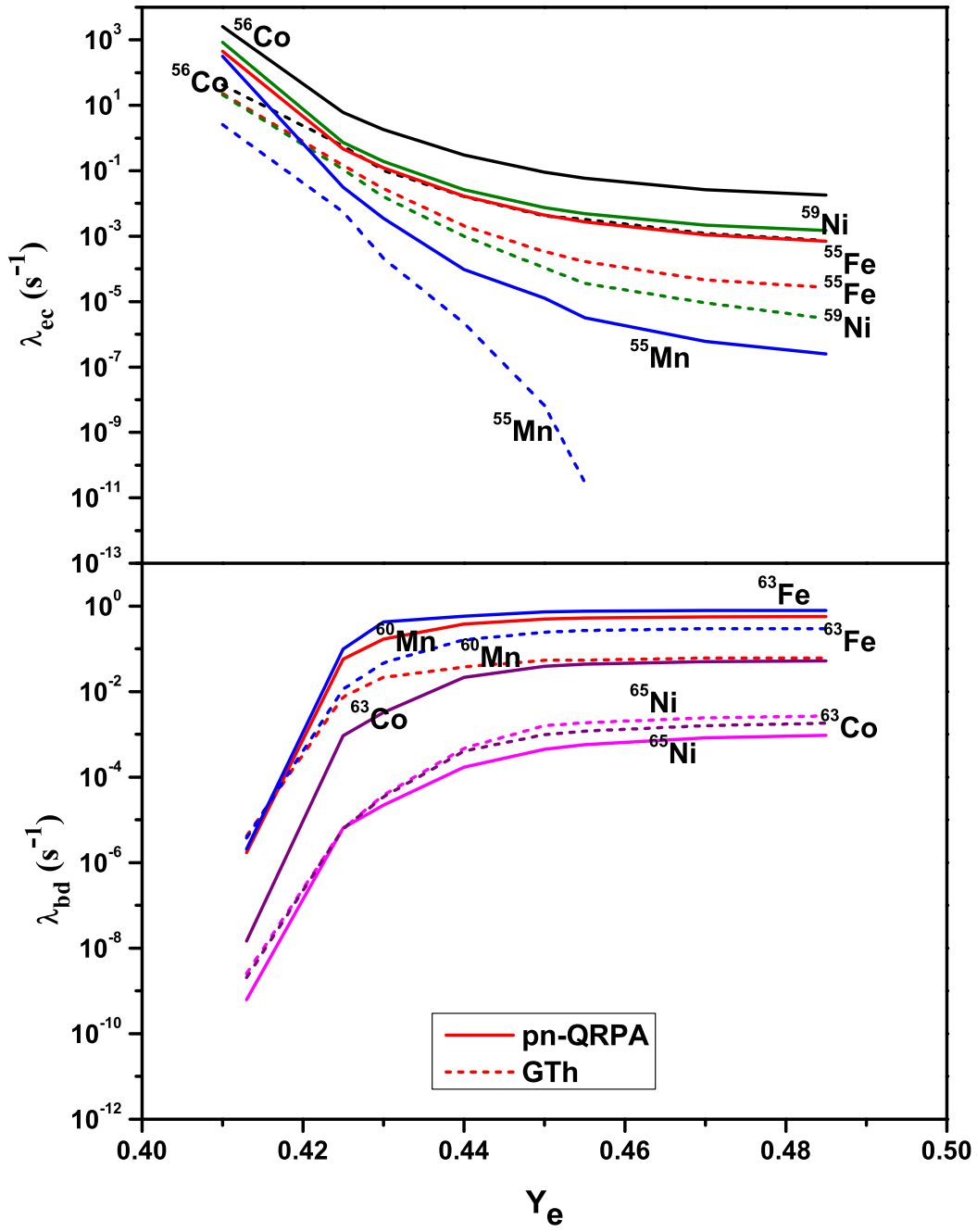


Figure 2. Comparison of the pn-QRPA and GTh weak decay rates as a function of Y_e .

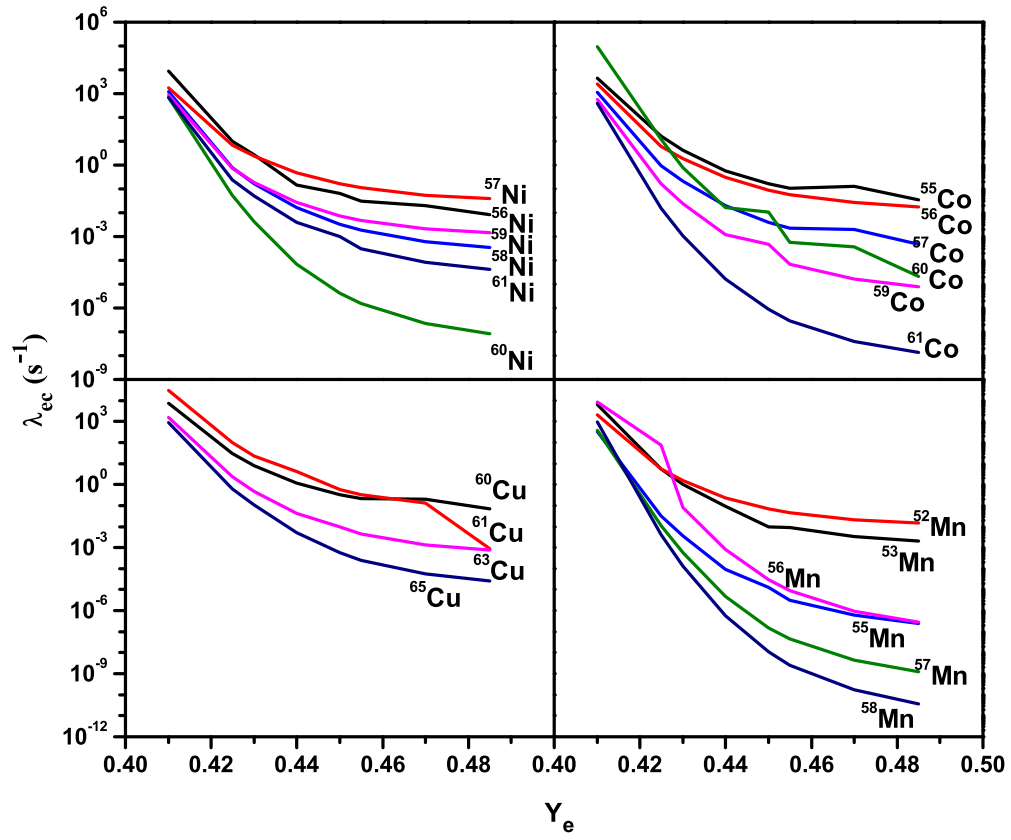


Figure 3. The pn-QRPA calculated ec rates as a function of Y_e for isotopes of Ni, Co, Cu and Mn.

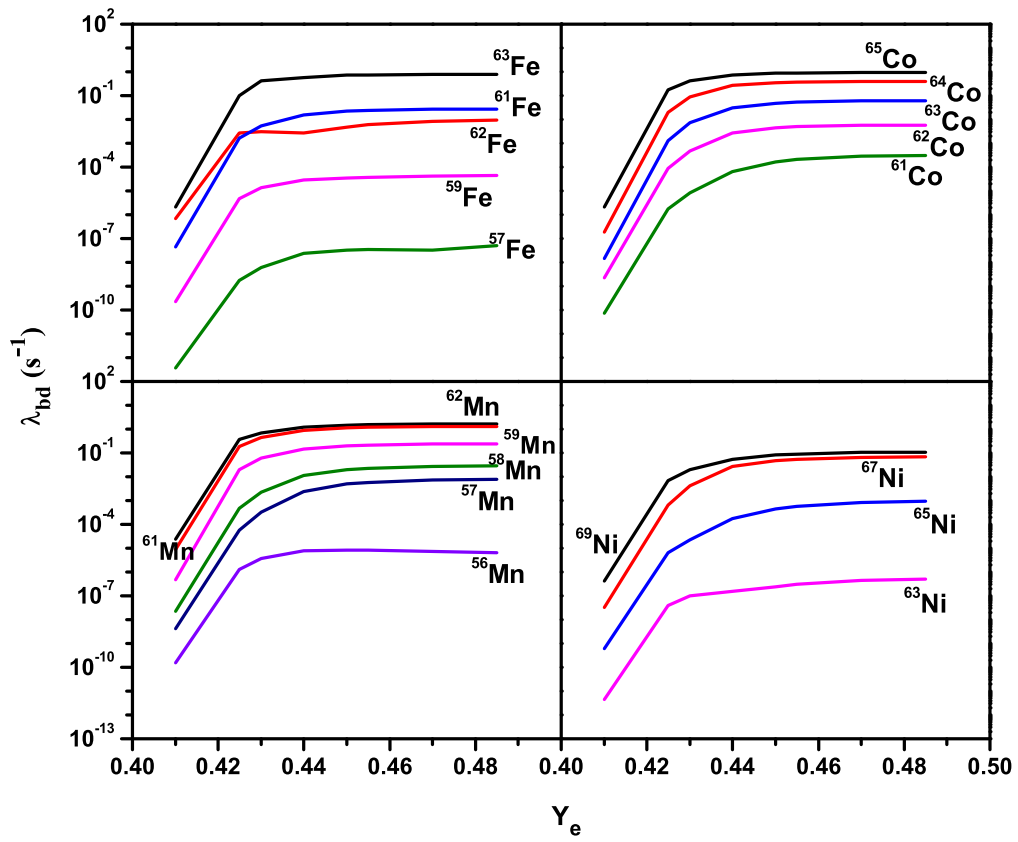


Figure 4. The pn-QRPA calculated bd rates as a function of Y_e for isotopes of Fe, Co, Mn and Ni.

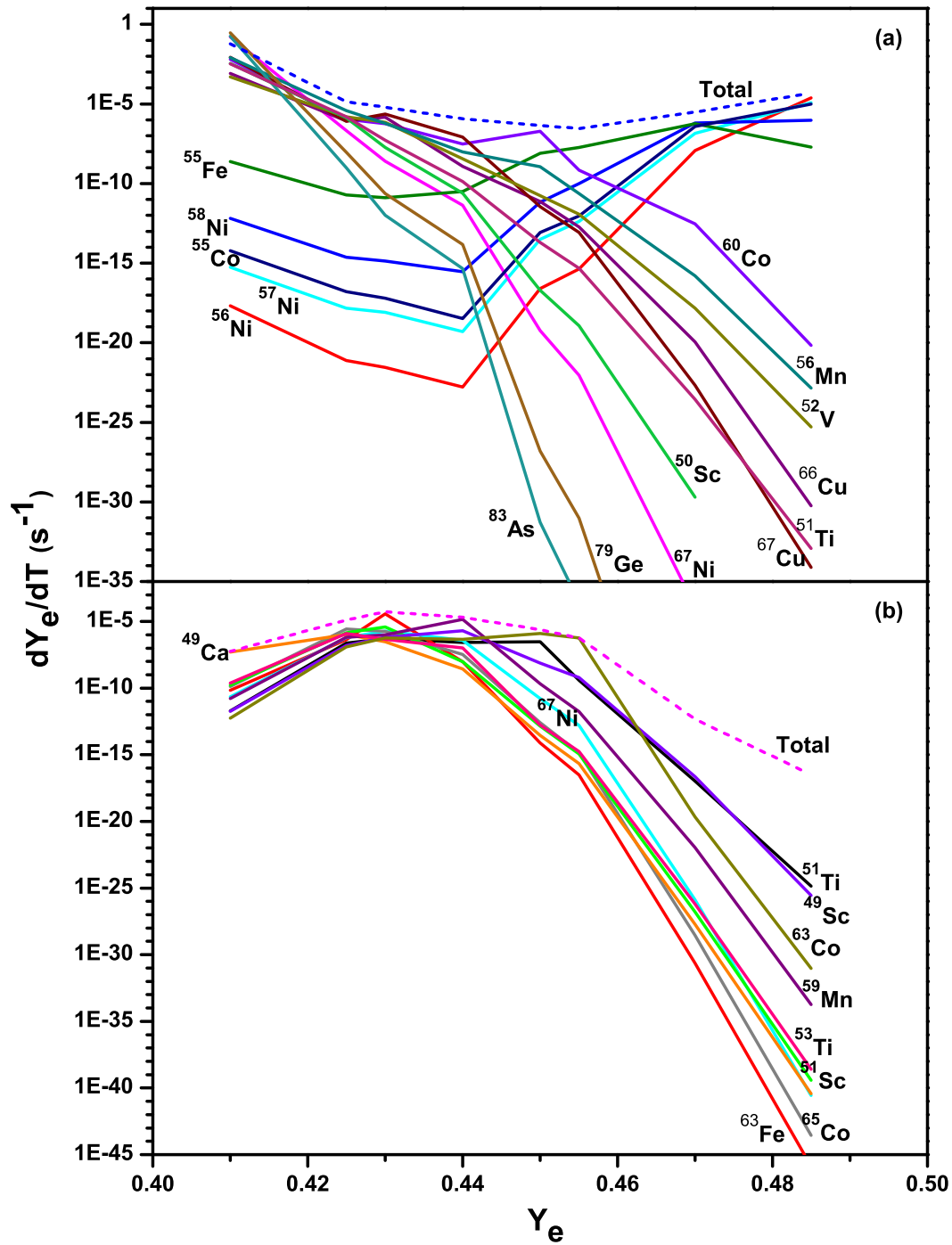


Figure 5. Evolution of temporal derivative of Y_e for (a) *ec* and (b) *bd* rates.

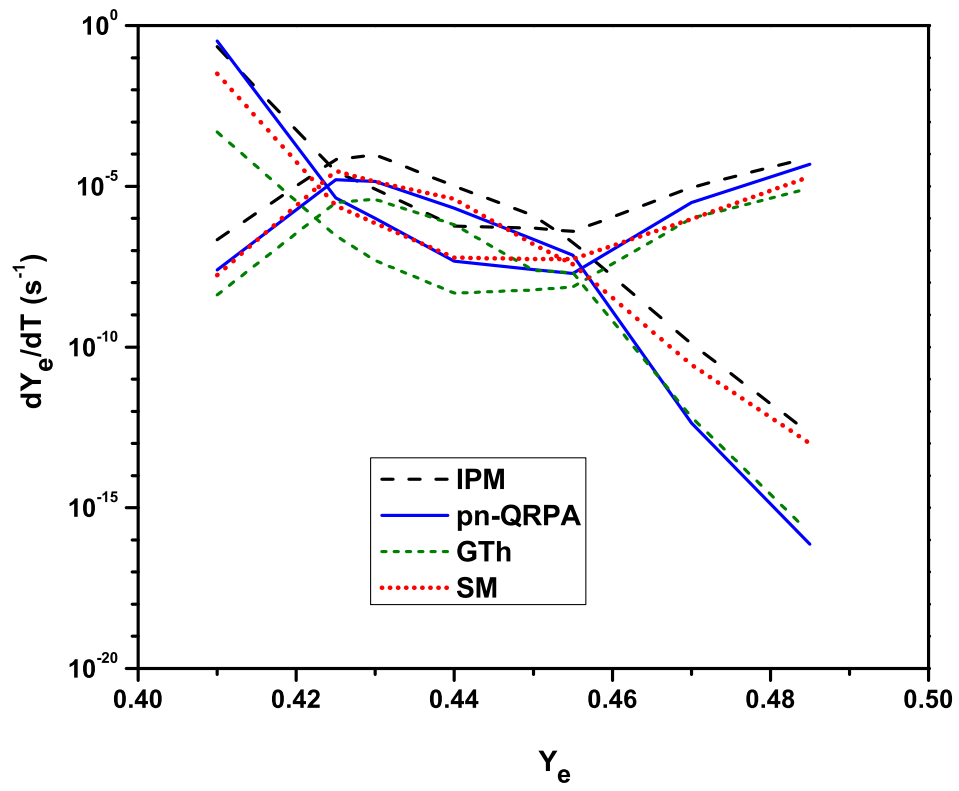


Figure 6. Competition between ec and bd in the evolution of Y_e .

REFERENCES

- Audi, G., Kondev, F., Wang, M., Huang, W., & Naimi, S. 2017, *Chinese physics C*, 41, 030001
- Aufderheide, M. 1991, *Nuclear Physics A*, 526, 161
- Aufderheide, M. B., Bloom, S. D., Resler, D. A., & Mathews, G. J. 1993a, *Physical Review C*, 47, 2961
- . 1993b, *Physical Review C*, 48, 1677
- Aufderheide, M. B., Fushiki, I., Woosley, S. E., & Hartmann, D. H. 1994, *The Astrophysical Journal*
- Bethe, H., Brown, G., Applegate, J., & Lattimer, J. 1979, *Nuclear Physics A*, 324, 487
- Bethe, H. A. 1990, *Reviews of Modern Physics*, 62, 801
- Brink, D. 1958, *Reports on Progress in Physics*, 21, 144
- Clifford, F., & Tayler, R. J. 1965, *Monthly Notices of the Royal Astronomical Society*, 129, 104
- Dimarco, A., Barbero, C., Dias, H., et al. 2002, *Journal of Physics G: Nuclear and Particle Physics*, 28, 121
- El-Kateb, S., Jackson, K., Alford, W., et al. 1994, *Physical Review C*, 49, 3128
- Ferreira, R., Dimarco, A., Samana, A. R., & Barbero, C. A. 2014, *The Astrophysical Journal*, 784, 24
- Fuller, G., Fowler, W., & Newman, M. 1982, *Astrophysical Journal Supplement Series*, 48, 279
- . 1985, *Astrophysical Journal*, 293, 1
- Fuller, G. M., Fowler, W. A., & Newman, M. J. 1980, *The Astrophysical Journal Supplement Series*, 42, 447
- Gove, N., & Martin, M. 1971, *Atomic Data and Nuclear Data Tables*, 10, 205
- Halbleib Sr, J. A., & Sorensen, R. A. 1967, *Nuclear Physics A*, 98, 542
- Hardy, J. C., & Towner, I. 2009, *Physical Review C*, 79, 055502
- Hartmann, D., Woosley, S., & El Eid, M. 1985, *The Astrophysical Journal*, 297, 837
- Heger, A., Woosley, S., Martínez-Pinedo, G., & Langanke, K. 2001, *The Astrophysical Journal*, 560, 307
- Hirsch, M., Staudt, A., Muto, K., & Klapdor-Kleingrothaus, H. 1993, *Atomic Data and Nuclear Data Tables*, 53, 165
- Juodagalvis, A., Langanke, K., Hix, W. R., Martínez-Pinedo, G., & Sampaio, J. M. 2010, *Nuclear Physics A*, 848, 454
- Kodama, T., & Takahashi, K. 1975, *Nuclear Physics A*, 239, 489
- Langanke, K., & Martínez-Pinedo, G. 2000, *Nuclear Physics A*, 673, 481
- Langanke, K., & Martínez-Pinedo, G. 2001, *Atomic Data and Nuclear Data Tables*, 79, 1
- Majid, M., & Nabi, J.-U. 2016, *Romanian Reports in Physics*, 68, 1447
- Majid, M., Nabi, J.-U., & Daraz, G. 2017, *Astrophysics and Space Science*, 362, 1
- Möller, P., Sierk, A. J., Ichikawa, T., & Sagawa, H. 2016, *Atomic Data and Nuclear Data Tables*, 109, 1
- Nabi, J.-U., & Bayram, T. 2020, *Astrophysics and Space Science*, 365, 19
- Nabi, J.-U., & Böyükata, M. 2016, *Nuclear Physics A*, 947, 182
- Nabi, J.-U., Cakmak, N., Stoica, S., & Iftikhar, Z. 2015, *Physica Scripta*, 90, 115301
- Nabi, J.-U., & Klapdor-Kleingrothaus, H. V. 1999, arXiv preprint nucl-th/9907106
- . 2004, *Atomic Data and Nuclear Data Tables*, 88, 237
- Nabi, J.-U., Tawfik, A. N., Ezzelarab, N., & Khan, A. A. 2016a, *Physica Scripta*, 91, 055301
- Nabi, J.-U., Tawfik, A. N., Ezzelarab, N., & Khan, A. A. 2016b, *Astrophysics and Space Science*, 361, 71
- Nakamura, K. 2010, *Journal of Physics G: Nuclear and Particle Physics*, 37
- Rauscher, T. 2003, *The Astrophysical Journal Supplement Series*, 147, 403
- Rauscher, T., & Thielemann, F.-K. 2000, arXiv preprint astro-ph/0004059
- Staudt, A., Bender, E., Muto, K., & Klapdor-Kleingrothaus, H. 1990, *Atomic Data and Nuclear Data Tables*, 44, 79
- Vetterli, M. C., Häusser, O., Abegg, R., et al. 1989, *Physical Review C*, 40, 559
- Weaver, T., Woosley, S., Fuller, G., et al. 1985, *Numerical astrophysics*, S
- Williams, A., Alford, W., Brash, E., et al. 1995, *Physical Review C*, 51, 1144